Please fill in the name of the event you are preparing this manuscript for.	SPE Improved Oil Recovery Conference
Please fill in your 6-digit SPE manuscript number.	SPE-200428-MS
Please fill in your manuscript title.	Polymer Retention Evaluation in a Heavy Oil Sand for a Polymer Flooding Application on Alaska's North Slope

Please fill in your author name(s) and company affiliation.

Given Name	Surname	Company
Dongmei	Wang	University of North Dakota
Chunxiao	Li	University of North Dakota
Randall S	Seright	New Mexico Tech

Abstract

For a polymer flooding field trial in a heavy oil reservoir on Alaska's North Slope, polymer retention is a key parameter. Because of the economic impact of retention, this parameter was extensively studied using field core material and conditions. Several important findings were noted. Polymer retention based on effluent viscosity measurements can be overestimated unless the correct (non-linear) relation between polymer concentration and viscosity is used. Polymer degradation (either mechanical or oxidative) can also lead viscosity-based measurements to overestimate retention. Inaccessible pore volume (*IAPV*) can be overestimated if insufficient brine is flushed through the sand between polymer banks. Around 100 pore volumes (*PV*) of brine may be needed to displace mobile polymer to approach a true residual resistance factor and properly measure *IAPV*. Even for a sand pack with k_{wsor} = 20 mD, *IAPV* was zero for HPAM with molecular weight (*Mw*) of 18 million g/mol. Fine-grain particles (<20 µm) strongly impacted polymer retention values. Native NB#1 sand with a significant component of particles <20 µm exhibited 290 µg/g, while the same sand exhibited 28 µg/g after these small particles were removed. Polymer retention did not necessarily correlate with mineral composition. The NB#1, NB#3, and OA sands had similar elemental and clay compositions, but the NB#1 sand exhibited ~10 times higher retention than the NB#3 sand. Polymer retention did not necessarily correlate with permeability. NB#1 sand exhibited much higher retention than OA sand, even though NB#1 sand was twice as permeable as OA sand. No evidence of chromatographic separation of HPAM molecular weights was found in our experiments. Although retention tended to be greater without a residual oil saturation (than at S_{or}), the effect was not strong. Aging a core (with high oil saturation) at 60°C reduced HPAM retention by a factor of two. As expected, under similar conditions, polymer retention was greater for a higher *Mw* HPAM (18 million g/mol) than for a lower *Mw* HPAM (10-12 million g/mol). In many cases with high polymer retention values (e.g., 240 µg/g), polymer arrival at the end of the core was relatively quick, but achieving the injected concentration occurred gradually over many pore volumes. This effect was not due chromatographic separation of polymer molecular weights. Results from modeling of this behavior was consistent with concentration-dependent polymer retention. The form assumed for the retention function in a simulator can have an important impact on the timing and magnitude of the oil response from a polymer flood. Field-based observations can underestimate polymer retention, depending on when the tracer and polymer concentrations were measured and the assumptions made about reservoir heterogeneity.

Introduction

This paper details the challenges encountered while determining polymer retention values for a polymer flooding pilot project in the Milne Point Schrader Bluff formation on the North Slope of Alaska. Details of this field project can be found in Dandekar *et al*. 2019,2020 and Ning *et al*. 2019. Previous work (Manichand and Seright 2014) demonstrated that low polymer retention values (e.g., < 50 μg/g) will generally result in only minor delays of the polymer bank, as it propagates through a formation. However, large polymer retention values (> 200 μg/g) can jeopardize the viability of a polymer flood. In this work, large retention values were noted for some sands and conditions, but not others.

Manichand and Seright (2014) extensively reviewed previous literature on retention and inaccessible pore volume (*IAPV*) prior to 2014. That review noted that clay and iron content in the rock or sand dominate polymer retention—implying the importance of grain surface area. Second, depending on the polymer type and molecular weight, polymer retention can increase dramatically with decreasing permeability, especially below 100 mD. However, most current polymer floods are applied in very permeable formations (greater than 500 mD). Third, most (but not all) data suggests that the Langmuir isotherm might not appropriately describe polymer retention. Fourth, retention of xanthan is usually significantly less than that of HPAM. Studies to 2014 suggest that polymer retention in the presence of residual oil was roughly half that in the absence of residual oil. Somewhat surprisingly, wettability had not been established as a key factor in polymer retention.

Since 2014, several additional papers on polymer retention were reported. Zhang and Seright (2014) noted that polymer retention can be relatively concentration independent at low concentrations, increase with increased concentration at intermediate polymer concentrations, and again insensitive to concentration at high concentrations. They proposed a mechanism where polymer orientation at the solid surface can explain these results. Zhang and Seright (2015) studied the relation between hydrodynamic retention and polymer rheology in porous media. Hydrodynamic retention was shown to have little effect on polymer rheology in porous media. Rodriguez *et al*. (2014) also noted that polymer concentration had a significant effect on polymer retention when displacing viscous oil. Ferreira and Moreno (2019) also studied the impact of polymer concentration on HPAM retention. Marliere *et al*. (2015) examined the use of a low-*Mw* HPAM in a surfactant flood in 1-2.5-mD rock. Wan and Seright (2017) noted that polymer retention under aerobic conditions could be twice as high as under anaerobic conditions. In contrast to previous counter-intuitive results, recent work by Wever *et al*. (2018) found retention on sand from an Oman reservoir to be more than 10 times less with oil present than without oil. Han *et al*. (2018) noted high retention values for hydrophobic associative polymers, compared with HPAM. Hou *et al*. (2018) introduced a new method for determining concentrations for nitrogen-containing polymers. Guetni *et al*. (2019) examined the effects of salinity, hardness and clay content and type on transport of a low-*Mw* HPAM in 50-100-mD sand packs. A number of authors recently studied polymer retention under conditions of high-temperature and/or high-salinity for applications in carbonate rock (Han *et al*. 2012, Gaillard *et al*. 2014, Quadri *et al*. 2015a,b, AlSofi *et al*. 2017, Fournier *et al*. 2018, Masalmeh *et al*. 2019, Alfazazi *et al*. 2018,2019, Seright *et al*. 2020)

In this paper, multiple types of laboratory measurements were used to assess HPAM polymer retention, including a brine tracer, effluent viscosity, total effluent organic carbon, and effluent chemiluminescent nitrogen. Retention tests were conducted in different Milne Point Schrader Bluff sands, with extensive permeability, grain size distribution, XRD, and XRF characterizations. Measurements were made both with and without residual oil present. HPAM samples with two different molecular weights were examined. The last part of this paper utilized analytical and numerical methods to assess effects of reservoir heterogeneity, polymer dispersion, and concentration-dependence of retention on the interpretation of the produced polymer and tracer values during field and laboratory applications.

Experimental Method

The Brine, Polymers and Polymer Solutions. The synthetic brine in this work was called Milne Point injection water, which contained 2435-ppm total dissolved solids (not including water of hydration)—consisting of 2173-ppm NaCl, 8-ppm KCl, 357-ppm $CaCl_2.2H_2O$, and 73-ppm $MgCl_2.6H_2O$. The calcium and magnesium salts were added as hydrates. This brine was passed through 0.45 μm Millipore filters before further use.

Two powder-form partially hydrolyzed polyacrylamides (HPAM) were used (both from SNF): Flopaam 3630S (Lot GJ1201, received from the Milne Point field application September 26, 2018) and Flopaam 3430S (Lot 3460). Nominal molecular weight values for the two polymers (based on intrinsic viscosity, given by the manufacturer) were 18 million g/mol and 10-12 million g/mol, respectively. The degree of hydrolysis was given as 30% for both polymers. **Figure 1** shows particle size distributions for these polymer powders, as determined using a Malvern Mastersizer 3000 with Aero-S dispersion unit (which uses laser diffraction to provide volume-based polymer-powder size distributions).

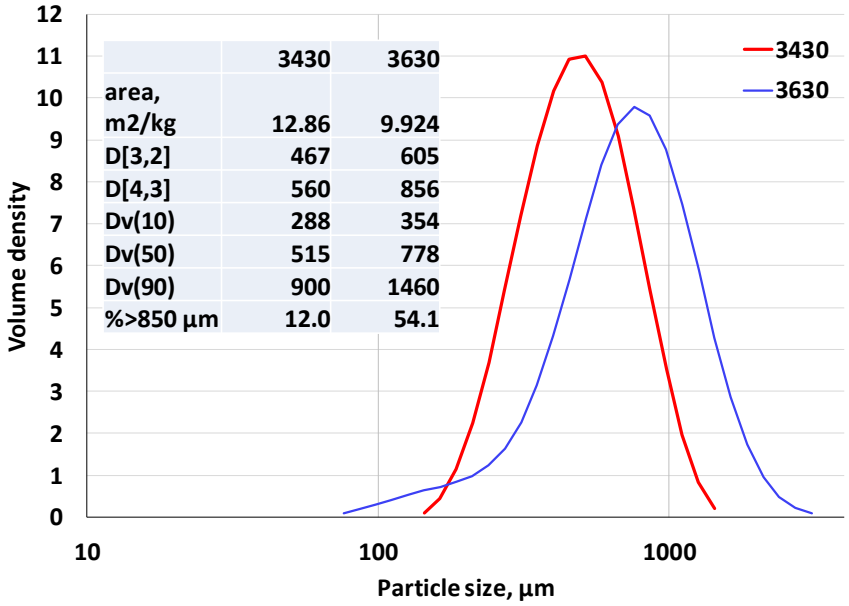

Figure 1—Particle size distributions for powder-form HPAMs.

Polymer solutions were prepared by sprinkling the appropriate mass of polymer powder (over the course of four minutes) onto the brine vortex created by an overhead stirrer (IKA Rw-200) at 300 rpm with a four-blade propeller. After initial mixing for several hours at high rate, the stir rate was reduced to ~100 rpm for at least two days. Polymer solutions were confirmed to be homogeneous by the absence of any lumps within a thin layer as the fluid flowed over a beaker lip when poured from one beaker to another. As in the field application, our target polymer solution viscosity was 45 cp (at 7.3 s^{-1} 25°C) For consistency, we fixed concentrations at 1750-ppm Flopaam 3630S and 2000-ppm Flopaam 3430S.

The Sands. Sand composition presumably plays a role in determining polymer retention. The Schrader Bluff sands of interest for the Milne Point polymer flood were the NB sand and the OA sand. The current polymer pilot is flooding NB sands, but OA sands are of high interest for expansion of the polymer flood. Our experiments used NB sands (provided by Hilcorp) from two different wells (located 3000 ft apart and at slightly different depths). We labeled NB sands from 3908 ft of the Pesado well as "NB#1"; and NB sands from 3757 ft of the Liviano well as "NB#3". The OA sand used in this work was from 4067 ft of the Pesado well. **Table 1** compares elemental compositions of the sands (as determined by X-ray fluorescence analysis with a Bruker Tracer 5g instrument with helium purge and Mudrock HE calibration). The sands are fairly similar in elemental composition, except the OA sand contains 5-7 times as much calcium, 30% more iron, and 30-100% more magnesium, and 70-90% less sulfur than the NB sands. The

NB#3 sand had 4-5 times as much sulfur as the NB#1 sand. **Table 2** lists X-ray-diffraction (XRD) analysis of the sands. The clay contents of the various sands were similar, with the NB#3 sand containing slightly less than the others. The OA sand contained noticeably more dolomite and feldspar (albite and orthoclase) than the NB sands.

Figure 2 compares the grain-size distributions for the two NB sands and the OA sand. These distributions were obtained using a laser-diffraction method (Malvern Mastersizer 3000 with Hydro EV dispersing unit), which provides volume-based measurements. The median grain size ranged from 96.6 µm for the OA sand to 166 µm for the NB#1 sand, and 382 µm for the NB#3 sand. The measurements provided estimates of average surface area of the sands (see the table in Figure 2). Interestingly, the OA and NB#1 sands had the same surface area (~93.5 m^2/g)—because the NB#1 sand contained a greater fraction of very fine material (<20 µm) that compensated for its larger average grain size. In contrast, the NB#3 sand had no grains smaller than 100 µm. Presumably, the fraction of very fine material significantly affected polymer retention. Polymer retention did not necessarily correlate with permeability (**Table 3**).

Table 1—Elemental analysis of sands (expressed in parts per million for the first 3 rows).

Element	Si	Al	Fe	K	Mg	Ti	Na	Ca	S	Ba	Mn	P	Zr	Zn	Sr	V
NB#1	168582	19537	18351	6043	2807	1914	1906	1756	804	542	257	140	89	59	54	48
NB#3	170713	15585	19063	4671	1901	1456	2053	2481	3542	454	143	180	247	115	167	119
OA	150396	18509	24720	6754	3714	2045	2357	12651	263	385	211	267	260	79	98	150
NB#1/NB#3	1.0	1.3	1.0	1.3	1.5	1.3	0.9	0.7	0.2	1.2	1.8	0.8	0.4	0.5	0.3	0.4
OA/ NB#1	0.9	0.9	1.3	1.1	1.3	1.1	1.2	7.2	0.3	0.7	0.8	1.9	2.9	1.3	1.8	3.1
OA/ NB#3	0.9	1.2	1.3	1.4	2.0	1.4	1.1	5.1	0.1	0.8	1.5	1.5	1.1	0.7	0.6	1.3

Table 2—XRD analysis of sands (expressed in percent).

	quartz	albite	orthoclase	dolomite	chlorite	illite	kaolinite
NB#1 original	86	10	0	1	1.5	1.5	0
NB#1 extracted (Pack 4)	86	10	0	1	1.5	1.5	0
NB#3 original	92	5	0	1	1	1	0
OA original	77	14	3	3	1.5	1.5	0

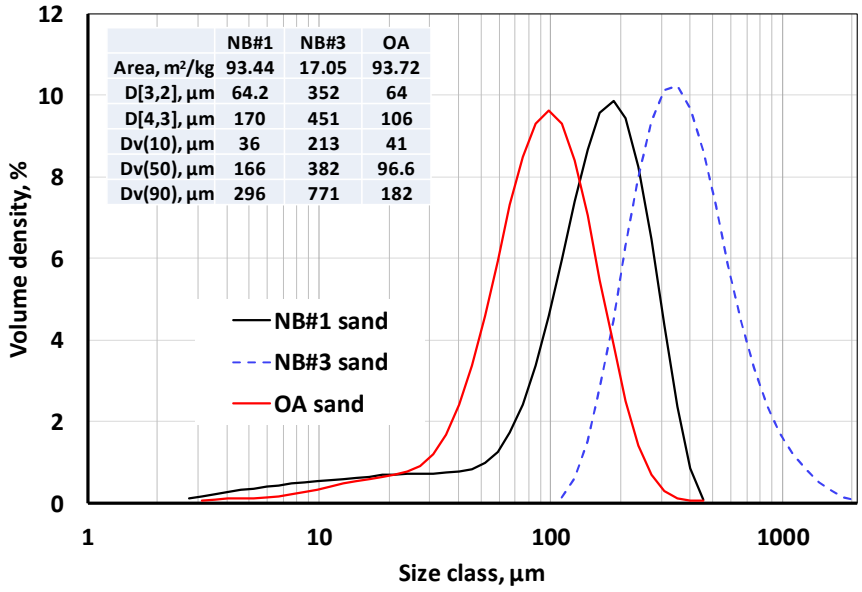

Figure 2—Grain-size distributions for the NB and OA sands.

Table 3—Summary of Polymer Retention Results

Pack	Sand	Polymer	k_{abs}, mD	k_w at S_{or}, mD	Pack length, cm	Sand cleaned?	Confining pressure, psi	Polymer retention, µg/g
1	NB#1	3630	11250	11250	60.1	no	0	290
2	NB#1	3630	6330	--	60.1	yes	0	153
3	NB#1	3630	9240	--	60.1	yes	0	170
4	NB#1	3630	10900	7000	60.1	Greatly	0	28
5	NB#1	3630	548	50	15.24	yes	1000	240
6	NB#1	3630	625	73	15.24	yes	1700	533
7	NB#1	3430	673	116	15.24	yes	1700	236
8	NB#3	3630	4100	4100	30.48	no	200	30
9	NB#3	3630	1778	1778	30.48	no	1000	32
10	OA	3630	233	19	15.24	yes	800	126
11*	OA	3630	470	20	30.48	yes	1000	65
12	OA	3630	158	--	15.24	yes	500	87
13	OA	3630	680	--	30.48	yes	500	56
14	OA	3430	328	--	15.24	yes	1000	0

* Pack 11 was aged for 6 days at 60°C at high oil saturation.

Sand Pack Preparation. Our sand packs were wet-packed. Our first four packs were 2 ft (60.96-cm) long, 1-cm diameter, and used no confinement pressure. Subsequent packs used a number of Temco Hassler core holders, including biaxial, triaxial, and with or without internal pressure taps. These were 1-inch diameter, and either 15.24-cm or 30.48-cm in length. To fine-tune the desired pack permeability, the confining pressure (i.e., overburden pressure) was varied (between 200 and 1700 psi). GE Druck DPI 104 pressure transducers were used—either 1000-psi transducers with 0.1 psi readout or 300-psi transducers with 0.01 psi readout. Four ISCO (Model 500D or 1000D) pumps were used during a typical experiment—one each for brine, polymer solution, oil, and confining pressure.

The condition of the sand varied, depending on the experiment. In some experiments (Packs 1, 8 and 9), the sand was used as received ("native state"). In other cases, the sand was washed/extracted with toluene and methanol and dried before use. In some cases, the sands were saturated only with brine before use. In other cases (Packs 4, 5, 6, 7, 10 and 11), the sand packs were flooded with fresh Milne Point oil (viscosity ~ 111 cp at 25°C) to connate water saturation, followed by flooding with at least 150 *PV* of brine to drive the sand pack to residual oil saturation. In one case (Pack 11), the sand pack was aged at high oil saturation for 6 days at 60°C before flooding to residual oil saturation and subsequent polymer retention determination. Table 3 summarizes the sand packs.

Flood Sequence and Polymer and Tracer Detection. After pack saturation, characterization, and stabilization of brine injection at a low rate (typically, 3.7 ft/d Darcy velocity), 5-13 *PV* of polymer solution were injected at a fixed rate, while monitoring pressure drops across the pack or pack sections.

Effluent from packs was analyzed by several methods. Routinely, we monitored a water tracer (20-ppm potassium iodide) using a Genesys 2 spectrophotometer at a wavelength of 230 nm. Effluent polymer concentration was monitored by three methods: total organic carbon, total nitrogen, and viscosity. For total organic carbon, a Shimadzu TOC-L was used. We recognize that this measurement might be influenced by the presence of any oil. Total nitrogen was measured using chemiluminescence with a Shimadzu TNM-L unit. Viscosity was measured at 7.3 s^{-1} (25°C) using proRheo LS-300 and/or Vilastic VE rheometers. The previous measurements were made at 3-4 cm^3 increments for each effluent sample. For selected samples, measurements of zero-shear viscosity were made (for estimation of intrinsic viscosity/molecular weight) using the proRheo LS-300 and/or Vilastic VE rheometers. For some samples, measurements of "particle size distribution" were attempted using a Malvern Ultrasizer for dynamic light scattering (at three angles: forward, back, and 90°).

Figure 3 illustrates the results during the first bank of polymer injection for a 30.48-cm-long pack with 4100-mD native-state NB#3 sand (Pack 8) with 200-psi confining pressure. This pack had one internal pressure tap that divided the pack into two equal sections. (Both sections had the same permeability.) To amplify the behavior near the time of polymer breakout, Figure 3 shows the first 2 *PV*

effluent (out of 5.4 *PV* total) of 1750-ppm Flopaam 3630S. All values are reported relative to the injected values. The dashed blue curve shows the tracer (KI) breakout. The black and green curves show breakout of the polymer, as judged by carbon content and nitrogen content, respectively. The solid red curve reports the specific reduced viscosity [(viscosity minus solvent viscosity)/ (solvent viscosity)] relative to the injected value. This red curve does not match up with the carbon and nitrogen curves because the relation between polymer concentration and solution viscosity is not linear. **Figure 4** illustrates this relation for Flopaam 3630S HPAM in Milne injection water. The equations in Figure 4 were used to convert effluent viscosities to polymer concentrations, and the dashed red curve in Figure 3 shows that these viscosity-based concentrations matched well with the carbon (black) and nitrogen (green) curves.

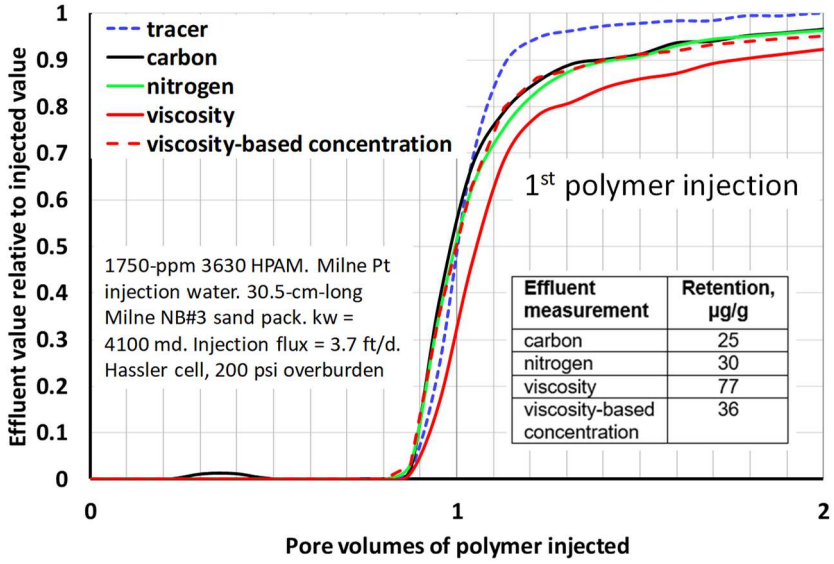

Figure 3—Effluent composition during the first polymer injection (4100-mD native NB#3 sand, Pack 8).

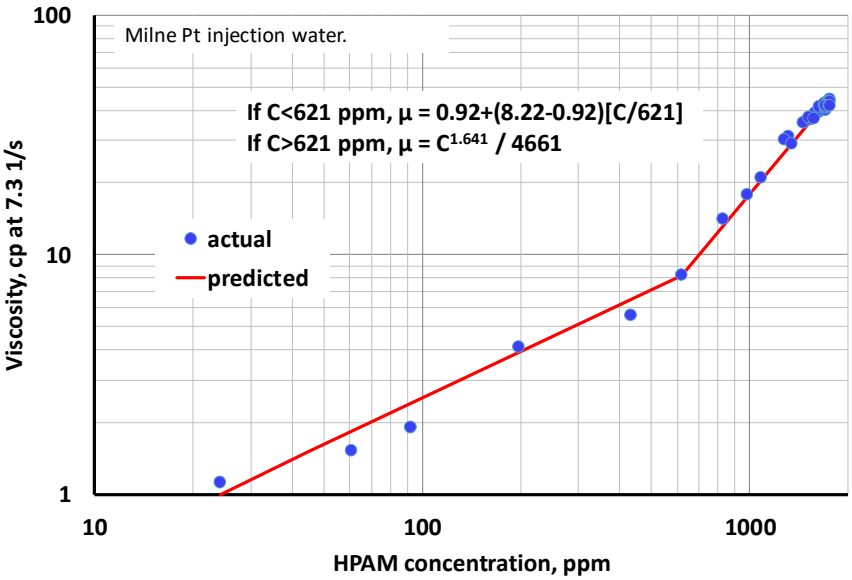

Figure 4—Viscosity versus concentration for Flopaam 3630S HPAM.

The difference in area between the tracer (dashed blue) curve and a given polymer curve in Figure 3 can be used to calculate polymer retention (if one assumes that inaccessible pore volume is zero). Specifically, Eq. 1 (from Manichand and Seright, 2014) provides a means for the calculations:

$$R_{pret} = \{[\Sigma\,[(C_{poly} * \Delta PV) - (C_{trac} * \Delta PV)]] + IAPV\} * PV / M_{rock} \quad (1)$$

where R_{pret} is polymer retention, C_{poly} is effluent polymer concentration, C_{trac} is effluent tracer concentration, PV is the volume in one pore volume, ΔPV is pore-volume increment, and M_{rock} is the rock mass in the sand pack.

Calculated polymer retention values were 25 μg/g based on effluent carbon, 30 μg/g based on effluent nitrogen, and 36 μg/g based on viscosity-based concentration. Within experimental error, these values may all be considered equivalent, with the nitrogen-based calculation representing the most reliable answer. Note that the incorrect assumption of viscosity being directly proportional to polymer concentration leads to a polymer retention value of 77 μg/g.

Inaccessible Pore Volume

Manichand and Seright (2014) reviewed previous petroleum literature for the phenomenon of inaccessible pore volume (*IAPV*). They noted that a limited number of inaccessible pore volume values were reported in the literature, and that the range of values reported is inconsistent, considering the conditions of the experiments. One might expect *IAPV* to increase with decreasing permeability and increasing HPAM molecular weight. However, **Table 4** (which compares several HPAM *IAPV* values from the literature) indicates no correlation between *IAPV*, permeability, and *Mw*.

Table 4—Literature *IAPV* values for HPAM.

Porous medium	*k*, mD	HPAM[1]	*Mw*, g/mol	*IAPV*, %	Reference
Berea	49-61	Pusher 500	3 million	17-37	Dabbous 1977
Berea	761	Pusher 500	3 million	19	Dabbous 1977
Berea	90-120	Pusher 700	5 million	0-4	Knight *et al* 1974
Berea	277	Pusher 700	5 million	18.7-24	Shah *et al*. 1978
Berea	470	Pusher 700	5 million	22	Dawson & Lantz 1972
Bartlesville	2090	Pusher 700	5 million	24	Dawson & Lantz 1972
Reservoir sand	30-453	Pusher 700	5 million	32-37	Vela *et al*. 1976
Teflon	86	Pusher 700	5 million	19	Dominguez & Willhite 1978
Sand pack	12600	Flopaam 3630S	18 million	35	Pancharoen *et al*. 2010

[1] All three HPAMs had 30% degree of hydrolysis.

Manichand and Seright (2014) point out that the available theories for the *IAPV* phenomenon cannot explain the magnitude and odd variations of *IAPV* with changes in permeability. It was noted the average diameter of an HPAM molecule in solution (~0.5 μm) is small enough that the polymer should be able to easily fit into over 99% of the pores present in typical polymer floods (Manichand and Seright, 2014).

We found a possible explanation for the inconsistent reports of inaccessible pore volume in the literature. In particular, we suggest that previous studies used varying volumes of brine to flush polymer from the cores between the first and second cycles of polymer injection. (Determination of *IAPV* requires injection of a polymer bank, followed by a brine bank to flush out un-adsorbed polymer, followed by a second polymer bank that presumably will not experience further retention, Lotsch *et al*. 1985.) When brine displaces viscous polymer solution, viscous fingering will occur, and many (100 or more) *PV* of brine may be required to displace all free (un-adsorbed) polymer (Chen *et al*. 2016, Seright 2017). If insufficient brine is injected during this period, some of the pore space will still be occupied by free polymer that could eventually be displaced. In other words, that un-displaced polymer could be misinterpreted as *IAPV*. To investigate and demonstrate this possibility, consider **Figure 5**, which plots residual resistance factor versus *PV* during brine injection after polymer for two different sand packs. (In each case, the packs were 30.5-cm long, with an internal pressure tap at 15.24 cm. The reported residual resistance factors apply to the second section of the packs.) Residual resistance factor is defined as mobility during original brine injection (before polymer injection) divided by brine mobility after polymer is displaced. It is often considered the permeability reduction provided by adsorbed polymer. In Figure 5,

the blue curve plots residual resistance factors during brine injection for the case of the 4100-mD NB#3 sand pack mentioned in Figure 3. Note that the residual resistance factor was 4 after 5 *PV* of brine and 1.6 after 100 *PV*.

In **Figure 6**, the polymer breakouts (as judged by nitrogen content in the effluent) are plotted for three (~5 *PV*) polymer banks associated with the 4100-mD NB#3 sand pack. The black curve is identical to the green curve in Figure 3. The dashed blue curve was observed when a second bank of polymer was injected following a 5 *PV* bank of brine. After this second polymer bank, 100 *PV* of brine was injected. Subsequently, the red curve was obtained when a third bank of polymer was injected. Note that red curve exhibits a 50% effluent concentration at 1 *PV*—indicating zero *IAPV*. This finding is consistent with the earlier suggestion (Manichand and Seright, 2014) that the 0.5-µm-diameter polymer can penetrate into virtually all aqueous pore space. In contrast, the dashed blue curve suggests that the *IAPV* after 5 *PV* of brine injection was 4%—because the 50% concentration was achieved 4% *PV* earlier than the red curve. We suggest that this apparent 4% *IAPV* value after 5 *PV* of brine is an artifact that results because mobile (un-adsorbed, un-displaced polymer) remains (because of viscous fingering). When the second polymer bank was injected, the brine viscous fingers disappeared and the 4% remaining mobile polymer saturation (from the first polymer bank) was displaced and produced. If brine had been flushed to the true residual polymer saturation, the *IAPV* would have been zero—as indicated by the red curve.

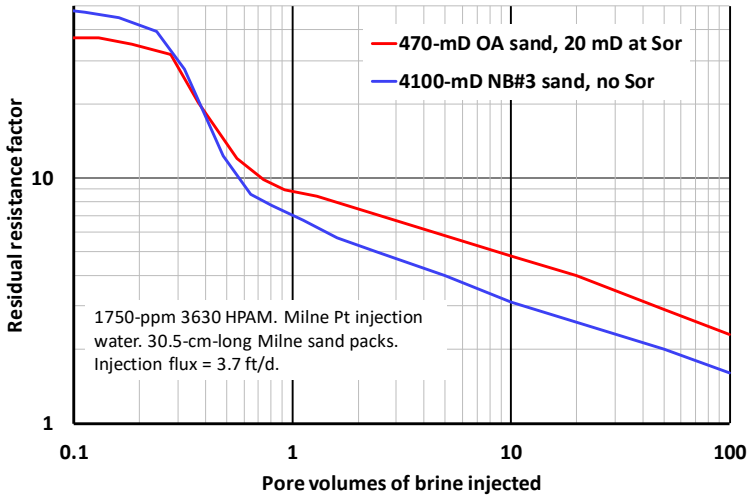

Figure 5—Residual resistance factors during 100 *PV* of brine injection (Packs 8 and 11).

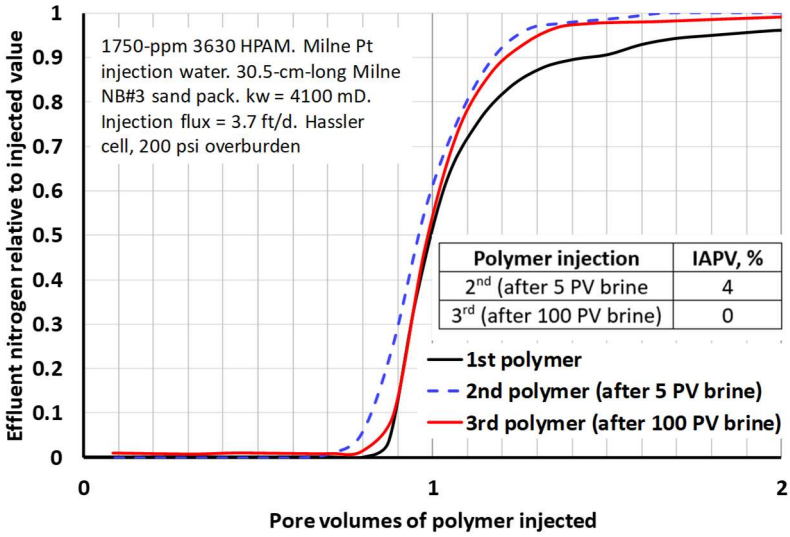

Figure 6—Nitrogen breakout during three polymer injections into 4100-mD NB#3 sand (Pack 8).

To further test this idea, another flood was performed involving a 470-mD OA-sand pack with a confining pressure of 1000 psi. After initial brine saturation, this pack was flooded to high oil saturation and then aged for 6 days at 60°C. The pack was then flooded with 150 *PV* of brine to reach residual oil saturation. Subsequently, the pack was flooded with 9.3 *PV* of 1750-ppm Flopaam 3630S HPAM. In **Figure 7**, the black curve shows the polymer breakout, while the green curve shows the tracer breakout during the first polymer injection into this sand pack. After polymer injection, 7 *PV* of brine were injected, ending with a residual resistance factor of 5.3. After this brine, a second bank of polymer solution was injected. In the dashed blue curve of Figure 7, the 50% effluent polymer concentration level (as judged by nitrogen chemiluminescence) was reached at 0.7 *PV* polymer injection—suggesting that the *IAPV* was 30%. Following this second polymer bank, 100 *PV* of brine were injected to drive the pack to a residual resistance factor (in the second pack section) of 2.3. At this point, a third bank of polymer solution was injected. For this case, the red curve in Figure 7 indicates that the *IAPV* was close to zero (because the 50% polymer concentration was reached at 1 *PV*). Thus, even in a porous medium with 20-mD permeability to water (i.e., 470-mD OA-sand at S_{or}), the polymer appears to access all the aqueous pore space. These examples illustrate how incomplete flushing of mobile polymer solutions (during a brine post-flush) can be misinterpreted as *IAPV*. For the remainder of this paper, we assume that inaccessible pore volume is zero. For field applications of polymer flooding, we support the suggestion of Manichand and Seright (2014): "A conservative approach to design of a polymer flood would assume that *IAPV* is zero, especially in multi-darcy sands."

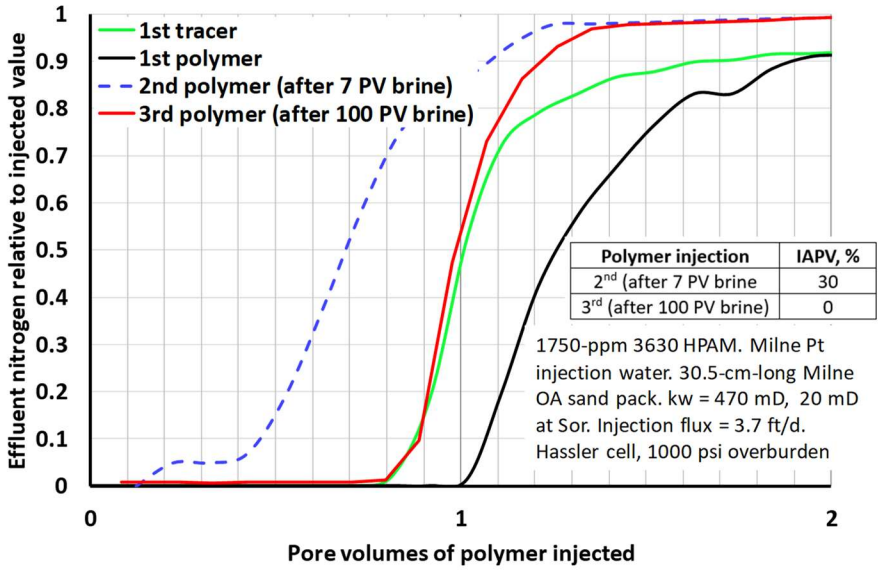

Figure 7—Nitrogen breakout during three polymer injections into 20-mD OA sand at S_{or}. (Pack 11)

Polymer Degradation during Propagation

In some cases, mechanical or oxidative degradation caused viscosity losses during the retention tests. Berge *et al*. (2018) also found that ion exchange can affect HPAM solution viscosities. In these cases, measurements based on viscosity greatly overestimate the degree of polymer retention. Fortunately, measurements based on total organic carbon and nitrogen chemiluminescence are not dependent on the degree of polymer degradation or viscosity loss.

Mechanical Degradation. Figure 8 shows mechanical degradation observed during the experiment associated with Figure 7—Flopaam 3630S in 470-mD OA sand (20 mD at S_{or}). The final pressure gradient during this experiment was about 1000 psi/ft (at 3.7 ft/d darcy velocity), so mechanical degradation was expected. After 4 *PV* of polymer injection, the effluent carbon (black), nitrogen (green), and tracer (blue)

concentrations were stable at the same values associated with the injected polymer solution. Also, the pressure drops across the two pack sections (solid grey and dashed grey curves) were equivalent and stable. And resistance factors in the two pack sections were fairly constant after 1 *PV* (see **Figure 9**)—in the range of 30 to 40 (values that were reasonably consistent with the injected viscosity values). However, the effluent viscosity (red curve) at 4 *PV* was 65% of the injected value—rising to 78% at 9 *PV*.

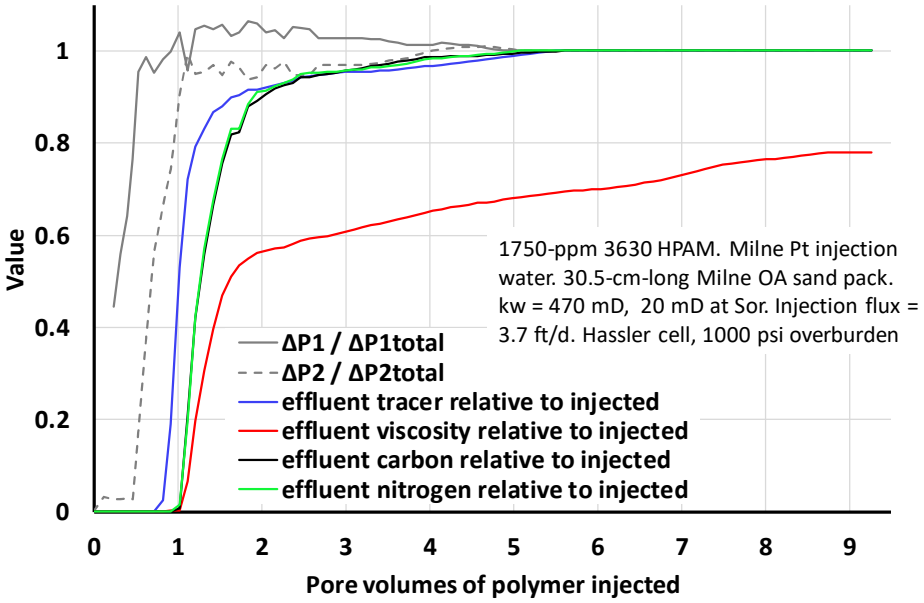

Figure 8—Mechanical degradation and viscosity loss during injection at 1000 psi/ft. (Pack 11)

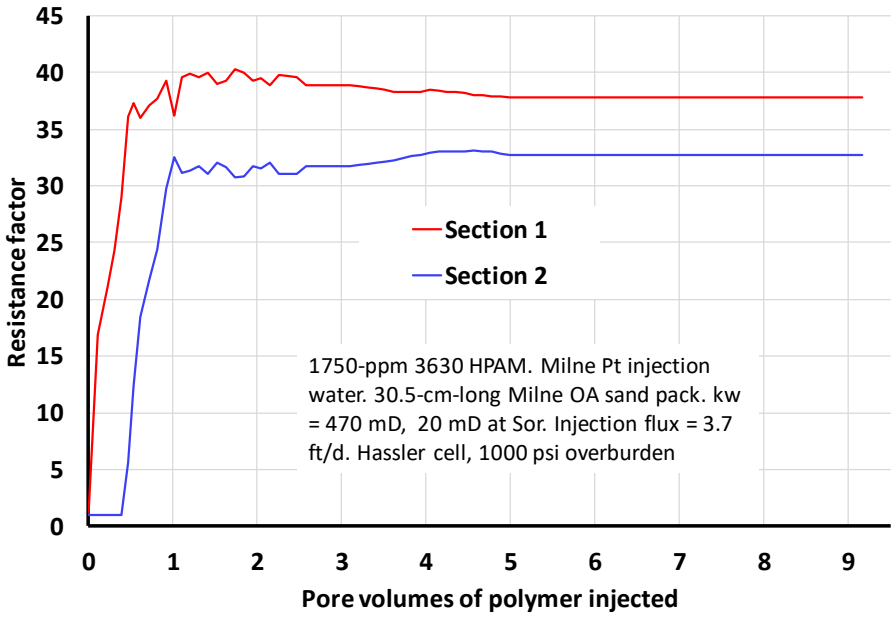

Figure 9—Resistance factors during polymer injection for the experiment in Figure 7. (Pack 11)

During this experiment, we also measured the zero-shear-rate viscosity (η_{zsr}) of each 3-4-cm^3 increment of effluent. This viscosity is the Newtonian plateau viscosity observed as shear rate approaches zero. This value is converted to the specific reduced viscosity (η_{spe}) by dividing η_{zsr} by the solvent viscosity, and then subtracting one. Jouenne *et al.* (2017) described a method to convert η_{spe} (which is unit-less) and polymer concentration (C, in g/L) to intrinsic viscosity ([η], in L/g) using Eq. 2.

$$\eta_{spe} = C\,[\eta] + 0.56\,(C\,[\eta])^{2.17} + 0.0026\,(C\,[\eta])^{4.72} \quad \text{.....(2)}$$

The Mark-Houwink relation can then be used to convert intrinsic viscosity to molecular weight (Eq. 3). In this case, we accept SNF's assignment of 18 million g/mol for the injected Flopaam 3630S HPAM (with intrinsic viscosity $[\eta]_1$). The Mark-Houwink exponent (a in Eq. 3) was taken as 0.76.

$$Mw_2 = Mw_1 ([\eta]_2 / [\eta]_1)^{(1/a)} \quad \text{.....(3)}$$

Based on this method, the blue curve in **Figure 10** plots effluent polymer Mw from ~1 PV to 9 PV. Effluent Mw values between 1 and 2 PV were relatively high, but these samples had the lowest effluent polymer concentrations and might have the greatest uncertainty in calculated Mw values. From 2 to 9 PV, the effluent Mw values increased slightly—from 12.6 to 14 million g/mol. Note in Figure 8 that the effluent polymer concentration was constant after 5 PV. Thus, the small increase in Mw was enough to raise the effluent viscosity (red curve in Figure 10) from 30.5 cp (at 5 PV) to 34.7 cp (at 9 PV).

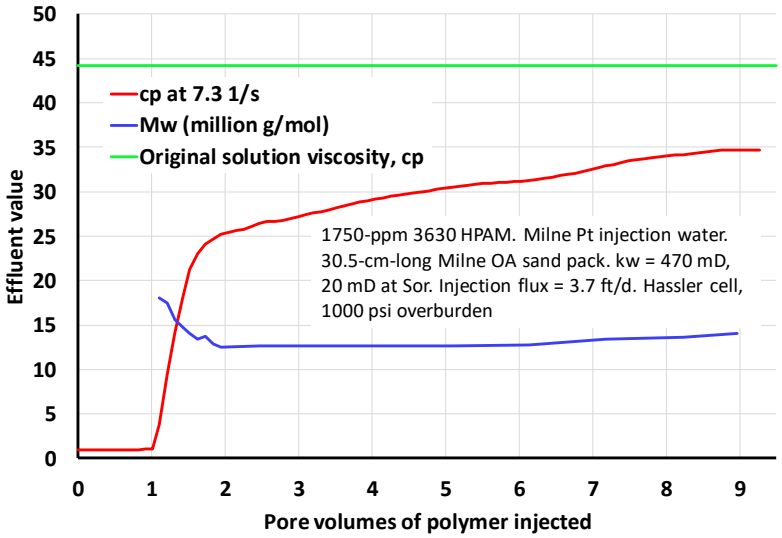

Figure 10—Molecular weights (based on intrinsic viscosity) of effluent associated with Figure 7. (Pack 11)

For this experiment, measurements of "particle size distribution" were also attempted using a Malvern Ultrasizer for dynamic light scattering (at three angles: forward, back, and 90°). The first measurements were made directly on the effluent samples—which had concentrations between 1500 and 1750 ppm. These concentrations were well above the polymer critical overlap concentration (C^*) for Flopaam 3630S in the Milne injection brine (i.e., about 250 ppm). Above C^*, the diffusion coefficient from dynamic light scattering dominantly measures motion associated with overlapping polymer segments—not with the rotation of individual polymer molecules. Not surprisingly, we could not distinguish any differences among any of the effluent samples. The instrument indicated that all the effluent samples had the same "particle size distribution", with a peak around 100 nm.

These effluent samples were then diluted to 200 ppm and re-measured using dynamic light scattering. Again, we could detect no difference among the various effluent samples. The samples were further diluted to 50 ppm, and again, no differences were detected using dynamic light scattering—even though concentrations were well below C^*. Our feeling is that this method is simply not sufficiently sensitive to detect differences in Mw for our HPAM polymers. Measurements of zero-shear-rate viscosity and intrinsic viscosity (i.e., using the method of Jouenne *et al*. 2017) gives a more reliable indication of Mw changes.

Oxidative Degradation. Our first two experiments used sand packed in steel tubes, with no confining pressure. Since dissolved oxygen was not excluded during our experiments, contact of the polymer with iron and oxygen could lead to oxidative degradation and polymer loss for some of these experiments. **Figure 11** illustrates this point for a 6330-mD NB#1 pack in a 2-ft-long steel tube (Pack 2 in Table 3).

The high permeability of this sand pack ensured that no mechanical degradation occurred. Nevertheless, the effluent viscosity stabilized at 91% of the injected value (i.e., a 9% viscosity loss)—presumably due to oxidative degradation. When this experiment was replicated in a plastic tube, the effluent viscosity stabilized at the injected viscosity (Pack 3 in Table 3). In subsequent experiments, as much as possible, flow lines were replaced with PEEK (polyether ether ketone) and contact with steel was minimized.

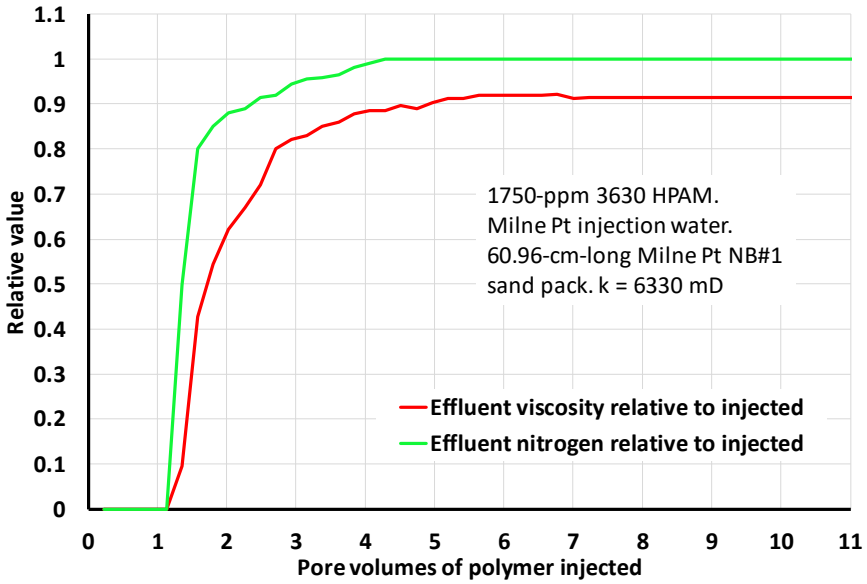

Figure 11—Oxidative degradation during polymer injection. (Pack 2)

Slow Rise in Effluent Polymer Concentration

Note in Figure 3 that about 60% of the polymer concentration broke out virtually simultaneously with the tracer—but then the effluent polymer concentration increased much more gradually than did the tracer. This result implies that polymer retention was effectively zero for this first component of polymer effluent, but another component of the polymer propagated more slowly. This observation is qualitatively consistent with the model of Zhang and Seright (2014), where polymer retention was suggested to be greater at high concentrations than at low concentrations. One might alternatively suggest that the "tailing" behavior was due to high-*Mw* parts of the polymer molecular-weight distribution traveling more slowly through the pack than low-*Mw* parts. To test this concept, we monitored the zero-shear-rate viscosity during the experiment described in Figure 3 and used the method of Jouenne *et al*. (2019) to convert these measurements to intrinsic viscosities and *Mw* (as was done in Figure 10). Within experimental error, we found no change in effluent polymer molecular weight throughout the course of injecting 5.4 *PV* of polymer. The effluent *Mw* values were the same as that for the injected polymer. Thus, we could not conclude that this sand pack caused chromatographic separation of HPAM by molecular weight.

Using the procedures mentioned in the discussion after Figure 10, dynamic light scattering was again used in an attempt to determine if polymer size and size distribution varied with effluent throughput. Again, the results revealed no detectable variations with *PV* throughput.

Figure 12 indicates that in 13 of 14 retention experiments (from Table 3), the effluent polymer concentration reached 60% of the injected value before injecting 1.4 *PV* of polymer solution. After that point, the rise in produced polymer concentration became more gradual, depending on the particular pack. For perspective, if the effluent concentration had reached the injected concentration at 1.4 PV, that would translate to a polymer retention of 88 μg/g. In other words, at least 60% of the polymer exhibits a retention value of 88 μg/g or less. The remaining polymer may exhibit higher retention—accounting for the higher retention values listed in Table 3 (especially for the NB#1 sand). A subsequent section will discuss the consequences of these observations.

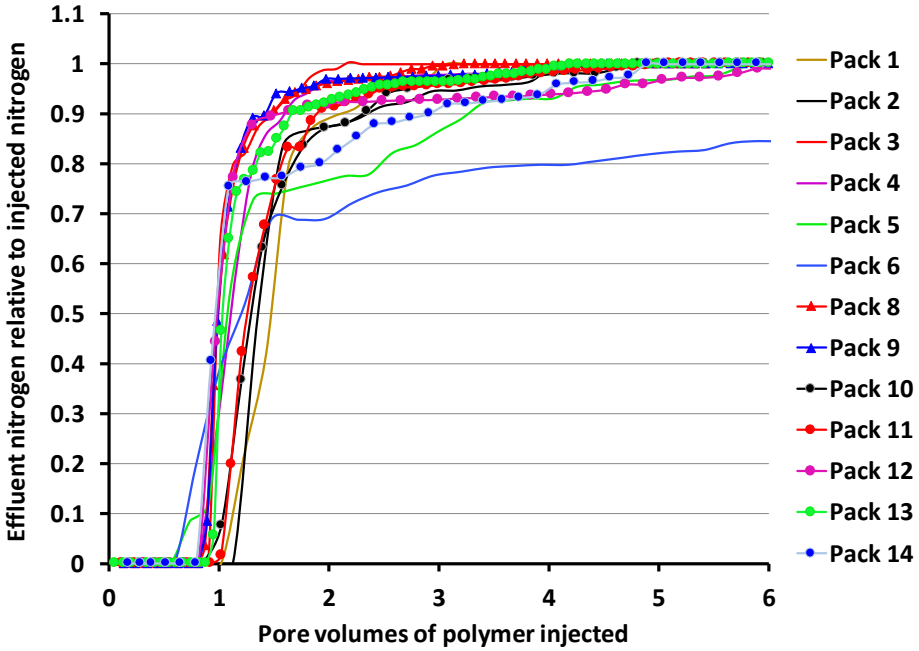

Figure 12—Tailing of effluent polymer concentrations.

Additional Polymer Retention Results

Table 3 provides a summary of the polymer retention results. In all these experiments, pressure drops across the sand pack stabilized within 2-3 *PV* of polymer injection, and no progressive plugging was observed (see Figures 8 and 9). Resistance factors were reasonably consistent with expectations based on viscosity measurements. Furthermore, at the end of every experiment, no polymer or gel accumulation was noted on any of the injection or production sand faces.

Several effects were examined during our retention studies, including sand type, pack permeability, residual oil, polymer molecular weight, and removal of the smallest particles from the sand.

Even though Table 1 indicates that the three sands (NB#1, NB#3, and OA) had similar elemental compositions, Table 3 reveals that polymer retention was lowest in the NB#3 sand (ranging from 30 to 32 μg/g). From Figure 2, note that NB#3 sand had the largest particles and no particles smaller than 100 μm. In spite of being from the same layer as NB#3 (except for being located 3000 ft away), polymer retention was highest in the NB#1 sand (153-533 μg/g, except for Pack 4 where 28 μg/g was observed). In the NB#1 sand, high retention values were noted even in very permeable packs (e.g., 290 μg/g with 11250 mD). As noted in Figure 2, the NB#1 sand had the most small particles (<20 μm). Retention values in the OA sand were intermediate (56-126 μg/g, except for Pack 14).

Prior to the retention experiment, the NB#1 sand in Pack 4 (exhibiting 28 μg/g retention) was extracted with toluene and methanol to a significantly greater extent than the other NB#1 sand packs in Table 3. This extraction process removed much more of the fine particles—explaining the low polymer retention value of 28 μg/g (red curve in **Figure 13**). In contrast, the NB#1 sand for Pack 1 (black curve in Figure 13) and the NB#3 sand for Pack 8 (dashed blue curve) were packed in their native state (no toluene or methanol extraction). All curves in Figure 13 were obtained by analyzing the sands after the retention experiment. For Pack 4 (red curve), after extensive cleaning/extraction, the pack was saturated with fresh Milne Point oil, and then driven to residual oil using 150 *PV* of brine. In contrast, for Packs 1 and 8, the native (naturally oil-coated) NB sands were packed and flooded without addition of fresh oil. Interesting, although the extensive extraction of Pack 4 removed substantial fines, it did not significantly change the clay or mineral content. The "NB#1 extracted" listing in Table 2 was from Pack 4 at the end of the flooding process. The XRD listings for that sand were identical to that for the native NB#1 sand.

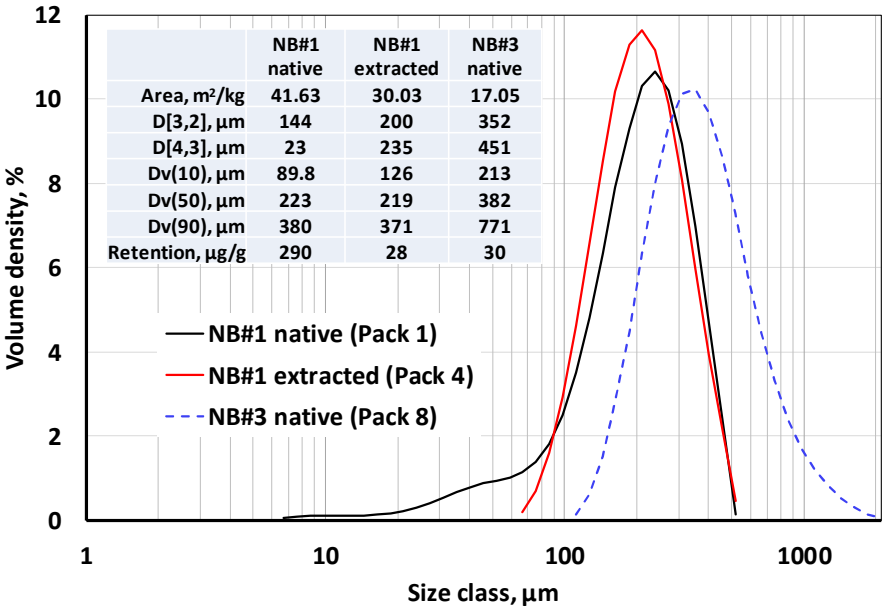

Figure 13—Grain size distributions for sands after retention experiments.

Within a given sand, polymer retention decreased modestly with increased permeability, but this was not a strong correlation (Table 3). For example, in the OA sand, retention in 233-mD sand (19-mD at S_{or}) was 126 µg/g, while retention in 680-mD sand (without residual oil) was 56 µg/g (Packs 10 versus 13).

Examination of Table 3 does not definitively reveal that retention was greatly lower with residual oil present than in oil-free packs. Comparison of Packs 10 and 11 (both with k_{wsor}=19-20 mD in the OA sand) suggest that aging the sand pack (at 60°C for 6 days at high oil saturation) may have reduced retention from 126 µg/g to 65 µg/g. This finding is consistent with findings of several previous studies (Manichand and Seright 2014). However, the result is counter-intuitive. One might expect that an oil coating on rock would dramatically reduce polymer retention, as observed by Wever *et al*. (2018).

Retention of Flopaam 3430S (with *Mw*=10-12 million g/mol) was lower than that of Flopaam 3630S (with *Mw*=10-12 million g/mol). For example, comparing Packs 6 and 7 indicates that under very similar conditions in the NB#1 sand, retention was 236 µg/g for 3430S versus 533 µg/g for 3630S. Similarly, comparing Packs 13 and 14 in the OA sands, retention was ~0 µg/g for 3430S versus 56 µg/g for 3630S. Mechanical entrapment is expected to be larger as HPAM *Mw* increases (Huh *et al*. 1990).

Effect of Heterogeneity on Field Determination of Retention

Reservoir heterogeneity can affect field-based measurements of polymer retention. Consider the case where a fracture allows direct channeling between an injector and producer. Polymer retention in this fracture will probably be low or zero, so that part of the flow stream may have no separation between the tracer and polymer fronts. In contrast, the part of the flow stream that passes through the porous rock should have a detectable difference between the tracer and polymer transit times.

For illustration, assume that the fracture/high-permeability channel accounts for 10% of the pattern pore volume, while homogeneous matrix accounts for the remaining 90%. Also assume that 50% of the flow that arrives at the production well travels through the fracture, while the other 50% travels through the matrix. Assume that polymer retention in the fracture is zero, but is 110 µg/g in the porous rock. Given a polymer concentration of 1750 ppm and matrix porosity of 0.25, this retention value means that the polymer bank in the matrix will travel 50% slower than the tracer bank. (See Eq. 1 of Manichand and Seright, 2014, to perform this calculation.)

For this scenario, **Figure 14** plots the expected concentrations of polymer and tracer in the produced water. Because retention is zero in the fracture, tracer and polymer breakthrough together after about 0.2

PV of polymer injection. If the field observations were stopped here, polymer retention would appear to be zero. If the concentrations were continued to be monitored up to 3 *PV* (of continuous polymer/tracer injection), another bank of tracer would appear to breakthrough about 1.8 *PV* and a second bank of polymer would break through about 2.6 *PV*. If the field data were then used to calculate polymer retention, a value of 55 µg/g would result—if the correct assumptions about reservoir heterogeneity were not made. Thus, field-based observations could result in a wide range of polymer retention calculations, depending on when the tracer and polymer concentrations were made and the assumptions made about reservoir heterogeneity.

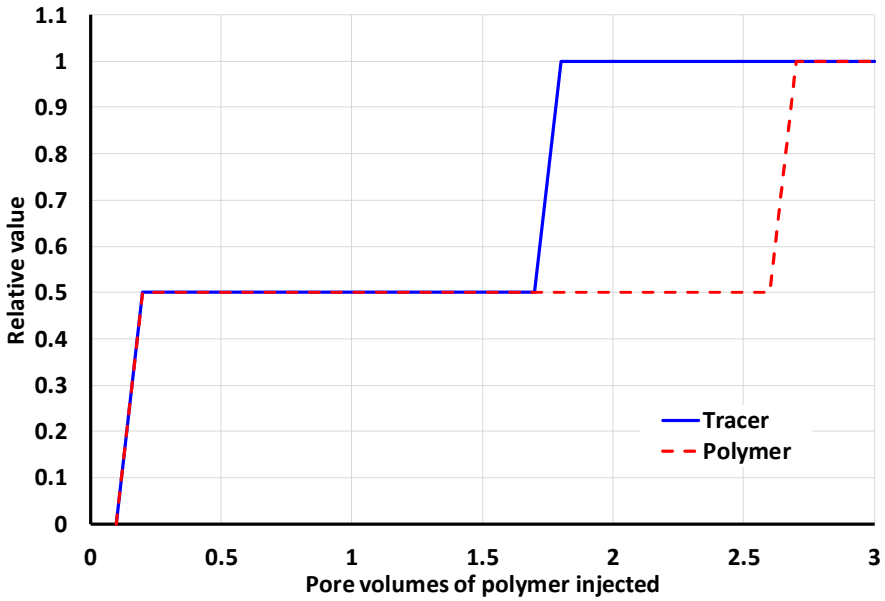

Figure 14—Effect of reservoir heterogeneity on field assessment of polymer retention.

Examination of Models of Polymer Retention

Simulators have options when treating polymer retention. Models often recognize that polymer adsorption is irreversible—i.e., once the polymer adsorbs onto the rock, it will not desorb under practical conditions. This discussion will not consider "hydrodynamic retention", which can be reversible. Hydrodynamic retention is typically only of interest at velocities seen near a well (Chauveteau and Lecourtier 1988, Zhang and Seright 2015).

The simplest model assumes that polymer retention is independent of concentration. In this case, once polymer enters a given grid block, no polymer will flow to the next grid block until the entire adsorption capacity of that first grid block has been satisfied.

A second, very common model of polymer (and other chemical) adsorption is the Langmuir isotherm:

$$R_{pret} = R_{pretmax}\, K_a\, C \,/\, (1+K_a\, C) \quad \text{.....(4)}$$

where $R_{pretmax}$ is the maximum allowable adsorption and K_a is a constant. This model predicts that some free (un-adsorbed polymer) will always exist once polymer enters a given grid block (until brine is injected after polymer). As a consequence, some polymer will always be available to flow to the next grid block. If ten grid blocks separate an injection well from a production well, the simulator may predict some low concentration of polymer at the production well after the tenth time step. This effect is an artifact, but it could be misinterpreted as supporting false positives associated with the clay flocculation test (for detection of produced polymer in a field application) that will be discussed in the next section.

A third model of polymer retention was introduced by Zhang and Seright (2014). They noted that polymer adsorption was constant at low concentrations (e.g., <100 ppm), increased with increased

polymer concentration at intermediate values (e.g., 100-1000 ppm), and was relatively constant at high concentrations (e.g., >1000 ppm). (A mechanistic explanation of this behavior can be found in their paper.) This model is qualitatively consistent with the observations in Figure 12. Some existing simulators can accommodate this behavior by allowing tabular input of polymer retention as a function of concentration.

As part of this work, CMG STARS and IMEX simulators were routinely used to model behavior in laboratory corefloods and in the field application. Details of this work will be presented in a future paper. Here, we briefly discuss some issues concerning use of the simulators to match our laboratory data.

Both STARS and IMEX could be made to approximate the observed laboratory retention data, although STARS consistently yielded greater dispersion of the polymer fronts. A false molecular mass must be used in the STARS modules because the actual polymer molecular weight (e.g., 18 million g/mol) will calculate extremely small polymer mole fractions (on the order of 10^{-9} or 10^{-10}), and then lead to numerical convergence difficulties. Even though the false polymer molecular weight reduces numerical convergence difficulties, differences in simulation results between using IMEX and STARS still exist. These differences may be acceptable for some analyses.

Figure 15 plots results from several attempts using IMEX to match the polymer breakout observed during the Pack-5 experiment listed in Table 3. Recall this experiment was performed in a 548-mD NB#1 sand pack, with k_w=50 mD at S_{or}. The solid circles in Figure 15 show the experimental results, based on nitrogen analysis of the effluent. The simulations were one-dimensional and had 61 grid blocks in the direction of flow. Other parameters in the simulation matched conditions of the experiment. The red curve shows the projected polymer breakout with a single retention input value in the model—specifically that retention is 240 µg/g if polymer concentration is 1750 ppm. This model assumes that polymer retention is zero at zero concentration, and that polymer retention increased linearly between zero and 1750 ppm. The red curve is fairly symmetrical and has the proper shape observed in some experiments—but not this one.

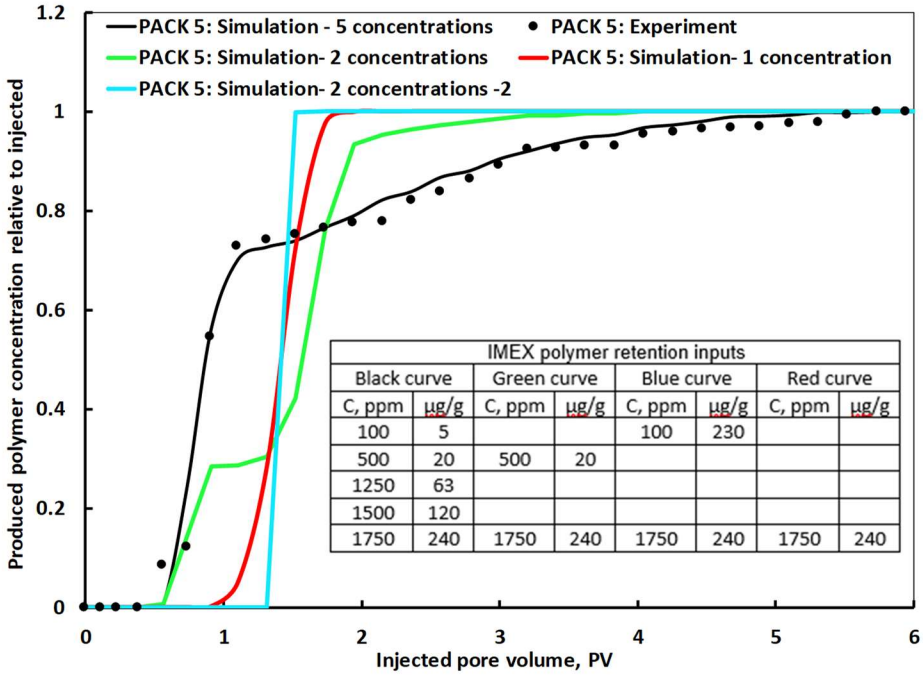

IMEX polymer retention inputs							
Black curve		Green curve		Blue curve		Red curve	
C, ppm	µg/g	C, ppm	µg/g	C, ppm	µg/g	C, ppm	µg/g
100	5			100	230		
500	20	500	20				
1250	63						
1500	120						
1750	240	1750	240	1750	240	1750	240

Figure 15—Attempted matches of Pack-5 polymer breakout using simulation.

The blue curve shows a projection with two retention inputs—specifically that retention is 230 µg/g at 100 ppm and 240 µg/g at 1750 ppm. Again, the simulator assumes that polymer retention is zero at zero concentration, and retention values are interpolated at intermediate concentrations. This case is close to an assumption that retention is independent of concentration. The blue curve is similar to the red curve, but is sharper (less dispersion).

The green curve also shows a projection with two retention inputs—specifically that retention is 20 μg/g at 500 ppm and 240 μg/g at 1750 ppm. The green curve shows rapid breakthrough of low-concentration polymer (~30% of injected value), followed by delayed breakthrough of higher concentrations.

The black curve uses five retention inputs, as listed in the table within Figure 15. Depending on concentration, retention values range from 5 μg/g to 240 μg/g. This set of inputs provides the closest match to the experimental data (the black circles).

All four of the simulations shown in Figure 15 are associated with 240 μg/g polymer retention. However, they will all predict different efficiencies of oil displacement. Cases associated with the blue and red curves predict a substantial delay (roughly double the time and polymer requirement) for an oil response as the case for zero retention. In contrast, the black curve (and the experimental data points) predicts timing and an oil response equivalent to injecting a polymer bank with zero retention, but with only 70% of the injected polymer concentration (i.e., a much faster response than from the blue and red curves, but with higher water cuts). The green curve predicts something intermediate. Thus, the form assumed for the retention input into a simulator can have an important impact on the timing and magnitude of the oil response from a polymer flood.

Produced Polymer from the Field Application

In the Milne Point polymer pilot project, about 7% PV of polymer solution (~45-cp Flopaam 3630S HPAM) was injected as of January 2020. Produced water samples from Milne Point Wells J-27 and J-28 have been monitored weekly for signs of polymer breakthrough and salinity changes (Ning *et al*. 2019 Dandekar *et al*. 2020). (Although since September, 2019, water cuts in Well J-28 have been so low that produced water samples have not been available.) Total organic carbon and nitrogen chemiluminescence were used to detect the presence of polymer, while atomic absorbance spectroscopy was used to monitor common cations (Na, K, Mg, Ca, Fe, Sr). As of January, 2020, no polymer was detected and no change in produced water composition occurred. **Figure 16** details results of polymer analysis of produced fluids (using a Shimizu TOC-L/TNM-L chemiluminescence instrument) for total nitrogen. (Recall that HPAM contains nitrogen.) Since November 2018, the produced fluids have contained, at most, the equivalent of ~20 ppm material that might (or might not) be polymer. This is a baseline amount which may be due to nitrogen compounds in the oil or to some other oilfield chemical that Hilcorp adds (perhaps corrosion inhibitor, biocide, scale inhibitor). It is not polymer, since it was present at the start of the project. If one wanted to argue that this concentration was due to HPAM, it would be equivalent to 1% of the injected HPAM concentration (as indicated in Figure 16).

About 10 months after the start of polymer injection, the field project noted that clay-flocculation tests showed positive for produced polymer. However, Figure 16 reveals that these clay-flocculation results are false positives (because the sensitive nitrogen-chemiluminescence test did not increase at that time). The clay-flocculation test is an easy, qualitative test that is convenient for field application, but it can give false positives due to interferences in the produced fluids (Lil *et al*. 2015). Any positive indication from the clay-flocculation test should be re-tested using a more reliable laboratory method—such as the chemiluminescence test, which has a normal limit of detection of 50 parts per billion (ppb) of nitrogen.

If one attempted to argue that 20-ppm HPAM was actually being produced, a credible explanation must be found to justify that. Since ~1750-ppm HPAM is injected, with a viscosity of 40-50 cp, that polymer solution should efficiently displace resident water in its path. So, when the polymer arrives at a production well, it might show a low concentration for a short time, but the concentration should rapidly rise to a value consistent with the flow contribution from the offset polymer injection well—i.e., at least, hundreds of ppm. A sustained produced polymer concentration of only 20 ppm is not credible based on any reasonable reservoir-engineering-based judgement. This further supports the fact that the clay-flocculation tests gave false positives.

Field-based estimates of polymer retention (such as those provided by Manichand and Seright, 2014) must await arrival of the polymer bank at the production wells.

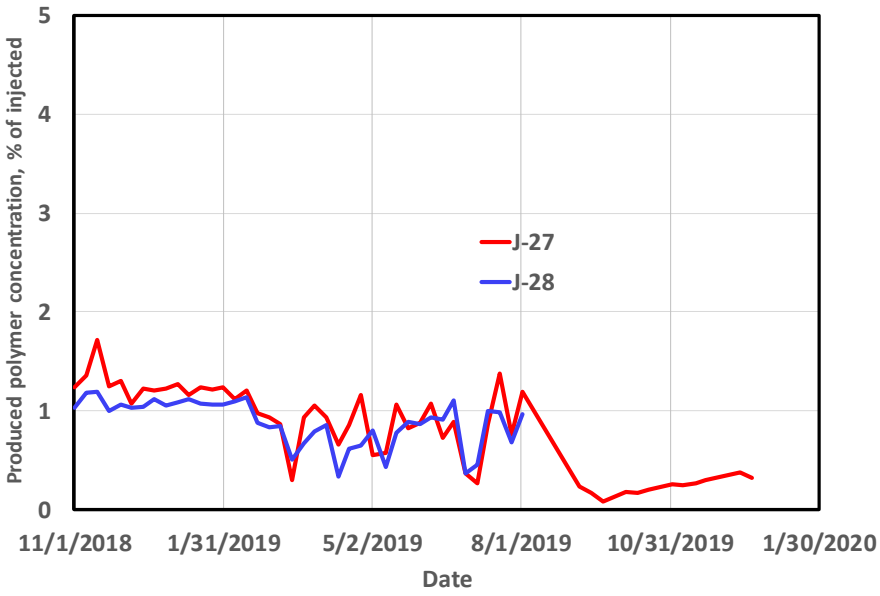

Figure 16—Analysis of polymer produced from Wells J-27 and J-28.

Conclusions

The following conclusions apply to a laboratory study of HPAM retention associated with a polymer flood in the Milne Point field on the North Slope of Alaska:

1. Polymer retention based on effluent viscosity measurements can be overestimated unless the correct (non-linear) relation between polymer concentration and viscosity is used. Polymer degradation (either mechanical or oxidative) can also lead viscosity-based measurements to overestimate retention.
2. Inaccessible pore volume can be overestimated if insufficient brine is flushed through the porous medium between polymer banks. Around 100 *PV* of brine may be needed to displace mobile polymer to approach a true residual resistance factor and properly measure *IAPV*. Even for a sand pack with k_{wsor} = 20 mD, *IAPV* was zero for HPAM with *Mw* of 18 million g/mol.
3. Fine-grain particles (<20 µm) strongly impacted polymer retention values. Native NB#1 sand with a significant component of particles <20 µm exhibited 290 µg/g, while the same sand exhibited 28 µg/g after these small particles were removed.
4. Polymer retention did not necessarily correlate with mineral composition. The NB#1, NB#3, and OA sands had roughly the same elemental and clay compositions, but the NB#1 sand exhibited ~10 times higher retention than the NB#3 sand.
5. Polymer retention did not necessarily correlate with permeability. NB#1 sand exhibited much higher retention than OA sand, even though NB#1 sand was twice as permeable as OA sand.
6. No evidence of chromatographic separation of HPAM molecular weights was found in our experiments.
7. Although retention tended to be greater without a residual oil saturation (than at S_{or}), the effect was not strong. Aging a sand pack (with high oil saturation) at 60°C reduced HPAM retention by a factor of two.
8. As expected, under similar conditions, polymer retention was greater for a higher *Mw* HPAM (18 million g/mol) than for a lower *Mw* HPAM (10-12 million g/mol).
9. In many cases with high polymer retention values (e.g., 240 µg/g), polymer arrival at the end of the sand pack was relatively quick, but achieving the injected concentration occurred gradually

over many pore volumes. This effect was not due chromatographic separation of polymer molecular weights. Results from numerical modeling of this behavior was consistent with concentration-dependent polymer retention. The form assumed for the retention function in a simulator can have an important impact on the timing and magnitude of the oil response from a polymer flood.

10. Field-based observations can underestimate polymer retention, depending on when the tracer and polymer concentrations were measured and the assumptions made about reservoir heterogeneity.

Acknowledgments

We thank Baojun Bai, Abhijit Dandekar, Samson Ning, Brent Sheets, Yin Zhang, and the rest of the team associated with Department of Energy Award Number DE-FE0031606 for interesting discussions. Thanks also to Hilcorp for providing the oil and core material used in this work. Thanks to Kate Wavrik for help in analyzing the produced water samples. XRD measurements were performed by New Mexico Tech's Bureau of Geology (Kelsey McNamara and Virgil Lueth).

"This material is based upon work supported by the Department of Energy under Award Number DE-FE0031606."

Nomenclature

a = Mark-Houwink exponent in Eq. 3
A_p = particle area, μm^2
C = polymer concentration, mg/L or ~ppm [μg/g]
C^* = polymer critical overlap concentration, mg/L or ~ppm [μg/g]
C_{inj} = injected polymer concentration during a retention study, mg/L or ~ppm [μg/g]
C_{poly} = produced polymer concentration, mg/L or ~ppm [μg/g]
C_{trac} = produced tracer concentration minus zero-baseline tracer concentration, mg/L or ~ppm [μg/g]
d_s = surface diameter, $(A_p/\pi)^{1/2}$, μm
d_v = volume diameter, $(6V_p/\pi)^{1/3}$, μm
$D[3,2]$ = Sauter mean diameter, d_v^3/d_s^2, μm
$D[4,3]$ = d_v^4/d_s^3, μm
$Dv(10)$ = particle diameter below which accounts for 10% of the material volume, μm
$Dv(50)$ = particle diameter below which accounts for 50% of the material volume, μm
$Dv(90)$ = particle diameter below which accounts for 90% of the material volume, μm
$IAPV$ = inaccessible pore volume
k = permeability, darcys [μm^2]
k_{wsor} = permeability to water at residual oil saturation, darcys [μm^2]
K_a = constant in the Langmuir isotherm (Eq. 4), L/mg
M_{rock} = mass of rock in the sand pack, g
M_w = polymer molecular weight, g/mol [daltons]
ΔP_1 = pressure drop across the first sand pack section, psi [Pa]
ΔP_2 = pressure drop across the second sand pack section, psi [Pa]

ΔP_{1total} = final pressure drop across the first sand pack section, psi [Pa]
ΔP_{2total} = final pressure drop across the second sand pack section, psi [Pa]
PV = pore volumes of fluid injected
ΔPV = pore volumes difference
R_{pret} = polymer retention, µg/g
$R_{pretmax}$ = maximum polymer retention in the Langmuir isotherm, µg/g
S_{or} = residual oil saturation
V_p = particle volume, μm^3
$[\eta]$ = intrinsic viscosity, L/g
η_{spe} = specific reduced viscosity
η_{zsr} = zero-shear-rate viscosity, cp [mPa-s]
ϕ = porosity
ρ_{rock} = rock density, g/cm^3

References

Alfazazi, U., AlAmeri, W., & Hashmet, M. R. 2018. Screening of New HPAM Base Polymers for Applications in High Temperature and High Salinity Carbonate Reservoirs. Paper SPE 192805 presented at the Abu Dhabi International Petroleum Exhibition & Conference held in Abu Dhabi, UAE, 12-15 November. http://dx.doi.org/10.2118/192805-MS.

Alfazazi, U., Thomas, N. C., AlAmeri, W., Al-Shalabi, E. W., and Shaik, A. R. 2019. An Experimental Investigation of Polymer Performance in Harsh Carbonate Reservoir Conditions. Paper 198607 presented at the SPE Gas & Oil Technology Showcase and Conference held in Dubai, UAE, 21-23 October. http://dx.doi.org/10.2118/198607-MS.

AlSofi, A. M., Wang, J., Leng, Z., Abbad, M., and Kaidar, Z. F. 2017. Assessment of Polymer Interactions with Carbonate Rocks and Implications for EOR Applications. Paper SPE 188086 presented at the SPE Kingdom of Saudi Arabia Annual Technical Symposium and Exhibition. Dammam, Saudi Arabia. 24-27 April. http://dx.doi.org/10.2118/188086-MS.

Berge. A.B.G.M. Lenchenkov, N., Wever, D.A.Z., Farajzadeh, R. Al-Mjeni, R., and Glasbergen, G. 2018. The Role of Synthetic Polymer on Rock-Fluid Interactions and the Resulting Slug for a cEOR Flood in the Sultanate of Oman. Paper SPE 190391 presented at the SPE EOR Conference at Oil and Gas West Asia. Muscat, Oman. 26-28 March. http://dx.doi.org/10.2118/190391-MS.

Chaveteau, G. and Lecourtier, J. 1988. Propagation of Polymer Slugs Through Adsorbent Porous Media. In *Water-Soluble Polymers for Petroleum Recovery*, eds. G.A. Stahl and D.N. Schulz, 53-68. Boston Massachusetts, Springer. http://dx.doi.org/10.1007/978-1-4757-1985-7_3.

Chen, Z., Du, C., Kurnia, I., Lou, J., Zhang, G., Yu, J., & Lee, R. L. 2016. A Study of Factors Influencing Polymer Hydrodynamic Retention in Porous Media. Paper SPE 179607. Presented at the SPE Improved Oil Recovery Conference. Tulsa, Oklahoma. 11-13 April. http://dx.doi.org/10.2118/179607-MS.

Dabbous, M.K. 1977. Displacement of Polymers in Waterflooded Porous Media and Its Effects on a Subsequent Micellar Flood. *SPE Journal* **17**(5) 358-368. SPE 6203-PA. http://dx.doi.org/10.2118/6203-PA.

Dandekar, A., Bai, B., Barnes, J., Cercone, D., Ciferno, J., Ning, S., … Zhang, Y. 2019. First Ever Polymer Flood Field Pilot - A Game Changer to Enhance the Recovery of Heavy Oils on Alaska's North Slope. Paper SPE 195257 presented at the SPE Western Regional Meeting. San Jose, California, USA, 23-26 April. http://dx.doi.org/10.2118/195257-MS.

Dandekar, A., Bai, B., Barnes, J., Cercone, D., Ciferno, J., Ning, S., … Zhang, Y. 2020. First Ever Polymer Flood Field Pilot To Enhance The Recovery Of Heavy Oils On Alaska'S North Slope - Pushing Ahead One Year Later. Paper SPE 200814 presented at the SPE Western Regional Meeting. Bakersfield, California, USA, 27 April-1 May. http://dx.doi.org/10.2118/200814-MS.

Dawson, R., and Lantz, R.B. 1972. Inaccessible Pore Volume in Polymer Flooding. *SPE Journal* **12** (5): 448–452. SPE 3522-PA. http://dx.doi.org/10.2118/3522-PA.

Dominguez, J.G. and Willhite, G.P. 1977. Retention and Flow Characteristics of Polymer Solutions in Porous Media. *SPE Jour*nal **17**(2) 111-121. SPE 5835-PA. http://dx.doi.org/10.2118/5835-PA.

Jouenne, S., Heurteux, G., Haorcq, C., Joly, M., Questrel, M., Levache, B. 2019. Universal Viscosifying Behavior of Acrylamide-based Polymers Used in EOR—Application for Aq/QC, Viscosity Predictions and Field Characterization. 20th European Symposium on Improved Oil Recovery. 8-11 April.

Ferreira, V. H. S., & Moreno, R. B. Z. L. 2019. Polyacrylamide Adsorption and Readsorption in Sandstone Porous Media. *SPE Journal* **preprint**: 1-18. http://dx.doi.org/10.2118/199352-PA.

Fournier, R., Tiehi, J. and Zaitoun, A. 2018. Laboratory Study of a New EOR-Grade Scleroglucan. Paper SPE 190451 presented at the SPE EOR Conference at Oil and Gas West Asia. Muscat, Oman. 26-28 March. http://dx.doi.org/190451-MS.

Gaillard, N., Giovannetti, B., Favero, C., Caritey, J.P., Dupuis, G., & Zaitoun, A. 2014. New Water Soluble Anionic NVP Acrylamide Terpolymers for Use in Harsh EOR Conditions. Paper SPE 169108. Presented at the SPE Improved Oil

Recovery Conference. Tulsa, Oklahoma. 12-16 April. http://dx.doi.org/10.2118/169108MS.

Gil, L., Gaillard, N., and Favero, C. 2015. Qualititative Determination of Polymer Presence by Flocculation. SNF Procedure QC-5065A. 16 October.

Guetni, I., Marliere, C., Rousseau, D., Bihannic, I., Pelletier, M., & Villieras, F. 2019. Transport of HPAM Solutions in low Permeability Porous Media: Impacts of Salinity and Clay Content. Paper SPE 195434 presented at the SPE Europec featured at 81st EAGE Conference and Exhibition held in London, England, UK, 3-6 June. http://dx.doi.org/10.2118/195434-MS.

Han, M., Zhou, X., Fuseni, A. B., Al-Zahrani, B. H., & AlSofi, A. M. 2012. Laboratory Investigation of the Injectivity of Sulfonated Polyacrylamide Solutions into Carbonate Reservoir Rocks. Paper SPE 155390 presented at the SPE EOR Conference at Oil and Gas West Asia. Muscat, Oman. 16-18 April. http://dx.doi.org/10.2118/155390-MS.

Han, X., Zhang, G., Yu, J., Chen, Z., & Kurnia, I. 2018. An Investigation of Retention and Unusually High Apparent Viscosity of Hydrophobically Associative Polymer in Porous Media. Paper SPE 190330. Presented at the SPE Improved Oil Recovery Conference. Tulsa, Oklahoma. 14-18 April. http://dx.doi.org/10.2118/190330-MS.

Hou, J., Han, M., & Fuseni, A. 2018. A Robust Nitrogen-Digestion Method to Determine the Concentrations of Polyacrylamide-Type Polymers. Paper SPE 192165. Presented at the SPE Kingdom of Saudi Arabia Annual Technical Symposium and Exhibition. Dammam, Saudi Arabia. 23-26 April. http://dx.doi.org/10.2118/192165-MS.

Huh, C., Lange, E.A., and Cannella, W.J. 1990. Polymer Retention in Porous Media. Paper SPE 20235 presented at the SPE/DOE Symposium on Enhanced Oil Recovery. Tulsa, OK. 22-25 April. http://dx.doi.org/10.2118/20235-MS.

Knight, B.L., Jones, S.C., and Parsons, R.W. 1974. Discussion. *SPE Journal* **14**(6) 643-644.

Lotsch, T., Muller, T., Pusch, G. 1985. The Effect of Inaccessible Pore Volume on Polymer Core Experiments. Paper SPE 13590 presented at the International Symposium on Oilfield and Geothermal Chemistry. Phoenix, AZ. 9-11 April. http://dx.doi.org/10.2118/13590-MS.

Manichand, R.N., and Seright, R.S. 2014. Field vs Laboratory Polymer Retention Values for a Polymer Flood in the Tambaredjo Field. *SPE Res Eval & Eng*. **17**(3): 314-325. http://dx.doi.org/10.2118/169027-PA.

Marliere, C., Wartenberg, N., Fleury, M., Tabary, R., Dalmazzone, C., & Delamaide, E. 2015. Oil Recovery in Low Permeability Sandstone Reservoirs Using Surfactant-Polymer Flooding. Paper SPE 177072 presented at the SPE Latin American and Caribben Petroleum Engineering Conference. Quito, Ecuador. 18-20 November. http://dx.doi.org/10.2118/177072-MS.

Masalmeh, S., AlSumaiti, A., Gaillard, N., Daguerre, F., Skauge, T., & Skuage, A. 2019. Extending Polymer Flooding Towards High-Temperature and High-Salinity Carbonate Reservoirs. Paper SPE 197647 presented at the Abu Dhabi International Petroleum Exhibition & Conference. Abu Dhabi, UAE, 11-14 November. http://dx.doi.org/10.2118/197647-MS.

Ning, S., Barnes, J., Edwards, R., Dunford, K., Eastham, K., Dandekar, A., … Ciferno, J. 2019. First Ever Polymer Flood Field Pilot to Enhance the Recovery of Heavy Oils on Alaska's North Slope - Polymer Injection Performance. Paper URTeC:643 presented at the Unconventional Resources Technology Conference. Denver, Colorado, USA. 22-24 July. http://dx.doi.org/10.15530/urtec-2019-643.

Osterioh, W.T., and Law, E.J. 1998. Polymer Transport and Rheological Properties for Polymer Flooding in the North Sea Captain Field. Paper SPE 39694 presented at the SPE/DOE Improved Oil Recovery Symposium. Tulsa, OK. 19-22 April. http://dx.doi.org/10.2118/39694-MS.

Pancharoen, M., Thiele, M.R., and Kovscek, A.R. 2010. Inaccessible Pore Volume of Associative Polymer Floods. Paper SPE 129910 presented at the SPE Improved Oil Recovery Symposium. Tulsa, OK. 24-28 April. http://dx.doi.org/10.2118/129910-MS.

Quadri, S. M. R., Jiran, L., Shoaib, M., Hashmet, M. R., AlSumaiti, A. M., & Alhassan, S. M. 2015a. Application of Biopolymer to Improve Oil Recovery in High Temperature High Salinity Carbonate Reservoirs. Paper SPE 177915 presented at the SPE Abu Dhabi International Peroleum Exhibition and Conference. Abu Dhabi, UAE, 9-12 November. http://dx.doi.org/10.2118/177915-MS.

Quadri, S. M. R., Shoaib, M., AlSumaiti, A. M., & Alhassan, S. M. 2015b. Screening of Polymers for EOR in High Temperature, High Salinity and Carbonate Reservoir Conditions. International Petroleum Technology Conference. http://dx.doi.org/10.2523/IPTC-18436-MS.

Rodriguez M., Rousseau, D., Bekri, S., Djabourov, M., & Bejarano, C. A. 2014. Polymer Flooding for Extra-Heavy Oil: New Insights on the Key Polymer Transport Properties in Porous Media. Paper SPE 172850 presented at the SPE International Heavy Oil Conference and Ehibition. Mangaf, Kuwait. 8-10 December. http://dx.doi.org/10.2118/172850-MS.

Shah, B.N., Willhite, G.P., and Green, D.W. 1978. The Effect of Inaccessible Pore Volume on the Flow of Polymer and Solvent through Porous Media. Paper SPE 7586 presented at the SPE Annual Technical Conference and Exhibition. Houston, TX. 1-3 October. http://dx.doi.org/10.2118/7586-MS.

Seright, R.S. 2017. How Much Polymer Should Be Injected during a Polymer Flood? Review of Previous and Current Practices. *SPE Journal* **22**(1): 1-18. http://dx.doi.org/10.2118/179543-PA.

Seright, R.S. Wavrik, K.E., Zhang, G., and AlSofi, A. M. 2020. Polymer Retention Evaluation in a Heavy Oil Sand for a Polymer Flooding Application on Alaska's North Slope. Paper SPE 200324 presented at the SPE Improved Oil Recovery Symposium. Tulsa, Oklahoma. 20-22 April. http://dx.doi.org/10.2118/200324-MS.

Vela, S., Peaceman, D.W., and Sandvik, E.I. 1976. Evaluation of Polymer Flooding in a Layered Reservoir with Crossflow,

Retention, and Degradation. *SPE Journal* **16** (2): 82–96. SPE-5102-PA. http://dx.doi.org/10.2118/5102-PA.

Wan, Hao, and Seright, R.S. 2017. Is Polymer Retention Different Under Anaerobic vs. Aerobic Conditions? *SPE Journal* **22**(2): 431-437. http://dx.doi.org/10.2118/179538-PA.

Wever, D. A. Z., Bartlema, H., ten Berge, A. B. G. M., Al-Mjeni, R., & Glasbergen, G. 2018. The Effect of the Presence of Oil on Polymer Retention in Porous Media from Clastic Reservoirs in the Sultanate of Oman. Paper SPE 190430 presented at the SPE EOR Conference at Oil and Gas West Asia. Muscat, Oman. 26-28 March. http://dx.doi.org/10.2118/190430-MS.

Zhang, Guoyin, and Seright, R.S. 2014. Effect of Concentration on HPAM Retention in Porous Media. *SPE Journal* **19**(3): 373-380. Paper 166256. http://dx.doi.org/10.2118/166256-PA.

Zhang, Guoyin, and Seright, R.S. 2015. Hydrodynamic Retention and Rheology of EOR Polymers in Porous Media. Paper SPE 173728 presented at the SPE International Symposium on Oilfield Chemistry. The Woodlands, Texas, 13-15 April. http://dx.doi.org/10.2118/173728-MS.

SI Metric Conversion Factors

cp x 1.0*	E-03	= Pa·s
ft x 3.048*	E-01	= m
in. x 2.54*	E+00	= cm
mD x 9.869 233	E-04	= μm^2
psi x 6.894 757	E+00	= kPa

* Conversion is exact.